

Aftershocks in Stress Shadows are Inconsistent with **Modeled Static Coulomb Stress Changes**

Jeanne L. Hardebeck (D * 1, Ruth A. Harris (D1





¹U.S. Geological Survey, Moffett Field, California, USA

Author contributions: Conceptualization: J. Hardebeck, R. Harris. Investigation: J. Hardebeck. Methodology: J. Hardebeck, R. Harris. Writing - original draft: J. Hardebeck. Writing – review & editing: J. Hardebeck, R. Harris.

Abstract Aftershock triggering is commonly attributed to increases in static Coulomb stress. In some areas, termed "stress shadows", a decrease in Coulomb stress is predicted to suppress earthquake occurrence. However, aftershocks are often observed in the modeled stress shadows. We examine several hypotheses that attempt to reconcile these shadow aftershocks with the static Coulomb stress change model: (1) they appear to be in shadows because of inaccuracy in the stress change calculations, (2) they occur on faults of unusual orientation which actually experienced increased Coulomb stress, (3) they occur on faults with different frictional properties, not modeled well by Coulomb stress, and (4) they are secondary aftershocks triggered by prior aftershocks or afterslip. When tested on the 2016 ${
m M_w}$ 7.0 Kumamoto, Japan, and 2019 ${
m M_w}$ 7.1 Ridgecrest, California, aftershock sequences, none of these hypotheses can explain the majority of the shadow aftershocks, and taken together these hypotheses can explain only about half of these aftershocks. This implies that Coulomb stress modeling that lacks small-scale fault zone heterogeneity might be inadequate to fully capture the true static stress changes and/or that other physical triggering models are needed, for example transient processes such as delayed triggering by dynamic stress changes from the passing seismic waves.

Non-technical summary Earthquakes usually trigger more earthquakes, referred to as aftershocks. The most widely accepted model for aftershock triggering is that they are caused by static stress changes in the Earth's crust generated by the mainshock. Stress changes are positive in some locations and negative in others. A persistent mystery is why some aftershocks occur in regions of stress decrease, called "stress shadows", where aftershocks are unexpected. We test four common hypotheses to explain these aftershocks: (1) modeling uncertainty, (2) incorrect assumptions about what faults the aftershock occur on, (3) incorrect assumptions about the physical properties of the faults, and (4) triggering by other aftershocks rather than the mainshock. Tested on two well-recorded earthquake sequences in Japan and California, we find that these hypotheses together can explain only about half of the aftershocks occurring in the stress shadows. This implies that our simple stress modeling calculation is inadequate to capture the true stress changes that occur in Earth's complicated crust, and/or that other triggering models are needed, for example triggering by the mainshock's seismic waves traversing the region.

Gareth Funning Handling Editor: Giuseppe Petrillo Copy & Layout Editor: Abhineet Gupta

Signed reviewer(s): Davide Zaccagnino Debi Kilb

Received: March 20, 2025 Accepted: September 28, 2025 Published: October 30, 2025

Introduction 1

Aftershock triggering is commonly attributed to the static Coulomb stress changes from the mainshock (e.g., Reasenberg and Simpson, 1992), "static" meaning the stress changes that persist after the passing of the seismic waves. The stress change tensor at a given location is usually computed in a simple elastic Earth model, and resolved onto a fault plane of a given orientation, called the receiver fault. The Coulomb stress change, ΔCS , is usually defined as:

$$\Delta CS = \Delta \tau + \mu(\Delta \sigma + \Delta p) = \Delta \tau + \mu' \Delta \sigma \tag{1}$$

where $\Delta \tau$ is the shear stress change in the slip direction of the receiver fault, $\Delta \sigma$ is the normal stress change on the receiver fault (tension positive), Δp is the change in pore fluid pressure, μ is the coefficient of friction, and μ' is the effective coefficient of friction (Reasenberg and Simpson, 1992). The equality on the right of Equation 1 is valid when Δp is proportional to $\Delta \sigma$. The actual fault planes of the aftershocks can be used as receiver planes, if known. Alternatively, the receiver faults are often chosen to be representative of the predominant local active fault orientations (e.g., McCloskey et al., 2003), or the optimally oriented faults in the total stress field (e.g., King et al., 1994). These two choices are often similar at distances of more than a few km from the mainshock.

A quantitative model of aftershock rate comes from combining the static Coulomb stress change with the rate- and state-dependent model of fault friction (Dieterich, 1994), called the Coulomb Rate and State (CRS) model (e.g., Stein et al., 1997; Harris and Simpson, 1998; Segou et al., 2013). The earthquake rate R at time t after a static Coulomb stress change ΔCS is:

^{*}Corresponding author: jhardebeck@usgs.gov

$$R(t) = \frac{R_{\text{back}}}{\left(\exp\left[\frac{-\Delta CS}{A\sigma}\right] - 1\right)\exp\left[\frac{-t}{t_a}\right] + 1}$$
(2)

where $R_{\rm back}$ is the background earthquake rate at the time of the stress change, t_a is the expected aftershock sequence duration given the tectonic stressing rate, and $A\sigma$ is a parameter that typically has values around 0.02 MPa. The integrated number of earthquakes N over the time period 0 to t is:

$$\begin{split} \frac{N}{N_{\rm back}} &= 1 + \frac{t_a}{t} \left[\frac{\Delta CS}{A\sigma} \right. \\ &\left. + \ln \left(\left(\exp \left[\frac{-\Delta CS}{A\sigma} \right] - 1 \right) \exp \left[\frac{-t}{t_a} \right] + 1 \right) \right] \end{aligned} (3) \end{split}$$

where $N_{\rm back}$ is the expected number of events at the background rate, $N_{\rm back}=tR_{\rm back}$.

For a negative ΔCS , the CRS model predicts a decrease in earthquake rate below the background rate, in regions referred to as stress shadows (Harris and Simpson, 1996). For negative ΔCS , assuming $|\Delta CS| >> A\sigma$, the integrated number of events over the time period 0 to $t << t_a$ is approximately:

$$\frac{N}{N_{\rm back}} \approx \exp\left(\frac{\Delta CS}{A\sigma}\right)$$
 (4)

This implies that a ΔCS of -1 MPa, on the order of typical earthquake stress drop, would cause a decrease in earthquake rate by more than 20 orders of magnitude. The CRS model therefore predicts, in the first days to weeks after a mainshock, an extremely low seismicity rate near the mainshock in the stress shadows.

The decrease in earthquake rate to below background that is predicted by the CRS model has been observed as regional decreases in moderate-sized events following M \sim 8 earthquakes (Harris and Simpson, 1996, 1998). However, the predicted rate decrease is generally not observed in aftershock sequences of moderate to large mainshocks (M=6-7.9). Seismicity rate decreases have been observed in a few cases where a modeled stress shadow overlaps an active aftershock area from a previous mainshock (e.g., Toda and Stein, 2003; Woessner et al., 2004; Toda et al., 2012), or where there is high background seismicity rate (e.g., Toda and Stein, 2022), where a decrease in rate is easier to observe than in lowseismicity rate regions (e.g., Marsan and Nalbant, 2005). However, most studies looking for stress shadows find only limited areas of rate decrease compared to the spatial extent of the modeled stress shadows (e.g., Marsan, 2003; Ma et al., 2005; Mallman and Zoback, 2007; Hardebeck and Harris, 2022), or conclude that there is no significant rate decrease at all (e.g., Felzer and Brodsky, 2005). Other studies find an initial increase in earthquake rate followed a few months later by a decrease below background rate (Toda and Stein, 2002; Ma et al., 2005; Marsan and Nalbant, 2005; Meng and Peng, 2014). Aftershocks in stress shadows may also contribute to the poor performance of Coulomb stress spatial kernels, compared to more isotropic kernels (Meade et al., 2017; DeVries et al., 2018; Sharma et al., 2020). These results suggest that earthquake occurrence in the stress shadows is not straightforward, and additional explanations might be required to fully explain the observed aftershocks.

There are several common hypotheses about what causes aftershocks to occur in the stress shadows, many of which attempt to reconcile these events with the static Coulomb stress triggering model:

- 1. All aftershocks occur in stress increase regions, but some appear to be in shadows because of inaccurate modeling, particularly of the mainshock source model and/or the receiver planes.
- 2. Aftershocks in stress shadows occur on faults with very different orientations from the optimally oriented or predominant fault orientations used as receiver faults, and instead occur on unusual planes receiving a positive ΔCS .
- The aftershocks in the stress shadows occur on faults with different frictional properties, which respond to changes in shear stress or changes in normal stress, rather than the combined effect in Coulomb stress.
- 4. Aftershocks trigger additional aftershocks, and the aftershocks in the stress shadows are secondary aftershocks triggered by static stress changes from prior aftershocks or by afterslip.

We test these hypotheses, using the aftershock sequences of the well-recorded 2016 M_w7.0 Kumamoto, Japan, and 2019 Mw7.1 Ridgecrest, California, earthquakes. We will focus on aftershocks occurring during the first two weeks following the mainshock, as this is when the aftershocks in the stress shadows appear most active (e.g., Hardebeck and Harris, 2022). We will consider aftershocks ≥4 km from the mainshock fault plane (median distance from the multiple mainshock rupture models), given the difficulties of modeling small-scale features of the static stress changes closer to the mainshock (e.g., Marsan, 2006). We will discuss the potential limitations on the modeling at distances ≥4 km due to small-scale features of the crust. We will also discuss the plausibility of alternative models, including triggering by dynamic stress changes (e.g., Kilb et al., 2000) and by post-seismic viscoelastic and poroelastic relaxation (e.g., Pollitz and Cattania, 2017; Beroza and Zanzerkia, 2024), and whether the aftershocks in the shadows could be continuing background earthquakes (e.g., Harris and Simpson, 1998).

2 Data and Methods

The Kumamoto and Ridgecrest earthquakes are chosen because both have at least 6 published finite-fault slip models that can be used to compute mainshock static stress changes. Using multiple finite-fault slip models allows us to characterize the uncertainty in the calculated stress change from the mainshock. Both regions are also covered by enhanced focal mechanism catalogs that allow detailed characterization of the predominant

active fault orientations and the fault planes of individual aftershocks.

2.1 Data

Finite fault models for the mainshocks were obtained from the SRCMOD Earthquake Source Model Database (Mai and Thingbaijam, 2014) and other publicly available sources. Kumamoto models are from Asano and Iwata (2016), Kubo et al. (2016), Kobayashi et al. (2017), Yagi et al. (2016), Yue et al. (2017), and Zhang et al. (2018). Ridgecrest models are from Barnhart et al. (2019), Jia et al. (2020), Jin and Fialko (2020), Liu et al. (2019), Ross et al. (2019), Xu et al. (2020), Yue et al. (2021), and Zhang et al. (2020). These models represent the complex mainshock fault geometries with different configurations of multiple planes. Coincidentally, both mainshocks were preceded by at least one large foreshock, a M6.2 and a M6.0 the day before the Kumamoto earthquake, and a M6.4 a day and a half before the Ridgecrest earthquake. Finite fault models for these M≥6 foreshocks are also obtained from the same sources, when available.

Aftershock locations are obtained from the Japan Meteorological Agency (JMA) catalog (Japan Meteorological Agency, 2024) for the Kumamoto earthquake and the Southern California Seismic Network (SCSN) catalog (California Institute of Technology and United States Geological Survey Pasadena, 1926) for the Ridgecrest earthquake. We consider aftershocks with M≥0 that are >4 km from the mainshock fault plane and within about 2 fault lengths of the mainshock (~85 km for Kumamoto and ~100 km for Ridgecrest, from Wells and Coppersmith, 1994). The median aftershock depth at Kumamoto is 8 km, with 90% of aftershocks occurring between 3 km and 12 km depth. The median aftershock depth at Ridgecrest (excluding the Coso geothermal field) is 5 km, with 90% of aftershocks occurring between 1 km and 14 km depth.

Focal mechanisms for aftershocks and background earthquakes are obtained from enhanced focal mechanism catalogs. For the Kumamoto sequence, we use A-C quality mechanisms from the focal mechanism catalog of Uchide (2020), and for the Ridgecrest sequence, we use A-C quality mechanisms from the focal mechanism catalog of Cheng et al. (2023), with additional restriction of azimuthal gap <120°, take-off angle gap <60°, and ≥8 observations to ensure that all mechanisms are well-constrained (e.g., Hardebeck and Shearer, 2002). For Kumamoto, the median magnitude of aftershocks with focal mechanisms is 2.1, with 90% between 1.6 and 3.1, and for Ridgecrest, the median magnitude is 1.8 and 90% are between 1.1 and 3.3. Focal mechanism uncertainty is reported for Ridgecrest, where median uncertainty is \sim 33°, with little correlation with magnitude below M2.5. Aftershocks with M≥2.5 exhibit slightly better constrained mechanisms with median uncertainty \sim 25°. The Kumamoto aftershocks show no correlation between magnitude and the assigned focal mechanisms quality metrics.

2.2 Methods

We use the finite-fault mainshock models to calculate the stress change tensor at receiver locations by modeling each mainshock as a set of dislocations in an elastic half-space (Okada, 1992). While an elastic half-space oversimplifies the structure of the crust, introducing additional structure such as a layered half-space does not appear to greatly improve Coulomb stress calculations (Sharma et al., 2020). The calculated Coulomb stress change does not include any smaller-scale structural features nor any non-elastic rheology, and for that reason it is an approximation of the true Coulomb stress change.

We define the background-fault stress change, $\Delta CS_{\mathrm{back}}$, as the calculated Coulomb stress change using the predominant active background faults as receiver planes. The receiver locations are the locations of aftershocks (M0-5.9) within the first 2 weeks of the mainshock, ≥4 km from the mainshock rupture, from the JMA and SCSN catalogs. Receiver fault orientations are inferred from the focal mechanisms of background earthquakes (occurring before the first foreshock). The predominant background mechanism is defined as the average mechanism of the closest 30 background earthquakes to a given aftershock, and the 1-sigma uncertainty is obtained from the RMS angular difference of the 30 mechanisms from this average. The median 3D receiver fault orientation uncertainty for Kumamoto is 32°, ranging from 10° to 58° depending on location, and the median for Ridgecrest is 36°, ranging from 20° to 52°.

We also compute the earthquake-specific Coulomb stress change, $\Delta CS_{\rm eq}$, for aftershocks within the first two weeks that have focal mechanisms in the Uchide (2020) or Cheng et al. (2023) catalogs. For these calculations, we use the locations and focal mechanisms of the aftershocks as the receiver locations and fault orientations. The 1-sigma mechanism uncertainty is taken directly from the Cheng et al. (2023) catalog, and for the Uchide (2020) catalog the mechanism uncertainty is translated from the letter quality (A=25°, B=35°, C=45°).

To quantify the uncertainty of the calculated Coulomb stress change, we perform 2000 realizations of the Coulomb stress calculation using different combinations of the multiple mainshock slip models, including or not including the M≥6 foreshocks, multiple choices of the receiver fault, and values of the effective coefficient of friction μ' between 0.2 and 0.8 (e.g., Reasenberg and Simpson, 1992). The receiver fault is randomly selected as one of the two focal mechanism nodal planes, of either the derived predominant background mechanism or the individual event mechanism. For each realization we randomly select one of the two nodal planes with equal probability, as the fault structure in both study areas is complex and either nodal plane is a plausible fault plane. The selected fault plane is then rotated about a random axis by an angle chosen from a normal distribution with zero mean and standard deviation equal to the mechanism uncertainty.

We define the probability that an aftershock experi-

enced a positive stress change, $P(\Delta CS)>0$, to be the fraction of realizations in which the calculated Coulomb stress change on the receiver fault is positive. We define the stress shadows as locations with a low probability of a stress increase on the background faults, $P(\Delta CS_{\rm back}>0)<1/3$, and the stress increase area as locations with a high probability of a stress increase, $P(\Delta CS_{\rm back}>0)>2/3$. For intermediate probabilities between 1/3 and 2/3, we consider the sign of the stress change to be ambiguous.

3 Results

3.1 Testing Hypothesis 1: Modeling Inaccuracy

One possible explanation for aftershocks in the stress shadows is that they appear there because of inaccuracy in the calculated Coulomb stress change, specifically due to uncertainty in the mainshock slip model or the choice of receiver faults. Hainzl et al. (2009) found that for the 1992 M_w 7.3 Landers, California earthquake, the slip model uncertainty resulted in a normal distribution of ΔCS values with a standard deviation of similar size to the mean, implying that it's not possible to confidently determine that any location is inside the stress shadow. A modification of the CRS model with this broad uncertainty has no areas of predicted seismicity rate decrease (Woessner et al., 2011), which performs well in testing but is not physically realistic because the actual mainshock must produce stress shadows somewhere. Different choices of receiver faults can also lead to different spatial distributions of stress increase and decrease (e.g., Steacy et al., 2005), further complicating the mapping of the stress shadow regions. This hypothesis only encompasses the modeling choices currently available for computing Coulomb stress change, and does not include possible effects from, for example, unmodeled fault zone heterogeneity.

We investigate the effects of modeling uncertainty by computing 2000 realizations of the background-fault stress change, $\Delta CS_{\rm back}$, and finding the probability of a positive stress change, $P(\Delta CS_{\rm back}>0)$. For both sequences, we find numerous aftershocks with high probabilities of occurrence in a stress shadow, i.e., $P(\Delta CS_{\rm back}>0)<1/3$. There are 355 of these shadow aftershocks (M=0-3.3) identified in the Kumamoto sequence, and 285 shadow aftershocks (M=0.3–3.7) in the Ridgecrest sequence (Figure 1). While any one of these events has some probability of having experienced a positive $\Delta CS_{\rm back}$, there is a very low probability that all of these events could have positive $\Delta CS_{\rm back}$. We conclude that many aftershocks fall in the stress shadows, even considering the impacts of modeling uncertainty.

Most of the shadow aftershocks occur adjacent to the mainshock rupture zone, while the aftershocks off either end of the rupture in the along strike direction tend to have a high probability of a stress increase (Figure 1). This is because a mainshock tends to increase stress on the continuation of the ruptured fault and generally relieves stress on subparallel planes, regardless of the details of the slip model. The spatial distribution of the

shadow aftershocks is different in detail between the two sequences. In the Kumamoto sequence (Figure 1a), the shadow aftershocks occur in a small cluster to the north of the mainshock rupture, and at the edges of the main aftershock clusters north of the northeast end of the rupture and south of the southwestern portion of the rupture. In contrast, the shadow aftershocks of the Ridgecrest sequence (Figure 1b) are scattered somewhat uniformly through areas east and west of the mainshock.

We can also compare the \sim 300 observed aftershocks in the stress shadows with the number predicted by the CRS model. Each realization of the Coulomb stress change calculation includes a stress shadow, and the size of the modeled shadow and the predicted number of aftershocks from the CRS model can be calculated. We perform 2000 realizations of the Coulomb stress change calculation on a 5-km-spaced grid spanning distances 4 to 25 km from the mainshock fault plane. Each realization uses a single mainshock source model, while the receiver fault orientation at each grid point is selected randomly from the distribution of background mechanisms at that location. The predicted number of shadow aftershocks for each realization is found by summing the predicted number of aftershocks in the grid cells of the modeled shadow for that realization, defined as all grid cells with negative ΔCS_{back} . The predicted number of aftershocks from the CRS model is calculated using Equation 3, with $A\sigma = 0.2 \,\mathrm{MPa}$. We calculate t_a from $t_a = A\sigma/\dot{\tau}$, where $\dot{\tau}$ is the background stressing rate (Dieterich, 1994). For Ridgecrest we use a stressing rate of $\dot{\tau} = 0.00027 \,\mathrm{MPa/yr}$, which was optimized to fit the CRS model to this sequence (Mancini et al., 2020). For Kumamoto we infer $\dot{\tau} = 0.0027 \,\mathrm{MPa/yr}$ from a strain rate of 90 nanostrain/yr (Sagiya et al., 2000). The background rate is estimated from the network catalog starting in 1981 (Ridgecrest) or 1983 (Kumamoto), using a minimum magnitude of M=2, and a b-value of 0.99 is used to extrapolate to the predicted number of M≥1 aftershocks.

The observed size of the stress shadow (defined as the set of grid cells where $P(\Delta CS_{\text{back}} > 0) < 1/3$) is smaller than the shadows in most of the model realizations (Figure 2), indicating that it is a conservative estimate of the stress shadow extent. Our definition of the stress shadow is roughly the intersection of multiple stress shadows computed with multiple different mainshock source models, which leads it to be smaller than the average size of the shadows of the individual mainshock models. The number of observed aftershocks in the stress shadow (\sim 300) is much larger than the number of aftershocks predicted by the CRS model in any of the modeled shadows, which ranges from <1 to 7 (Figure 2). We also identify the optimized stress shadow by finding the set of grid cells the size of the median modeled stress shadow that has the minimum number of aftershocks. These optimized stress shadows also have many more aftershocks than predicted by the CRS model in any of the realizations: 8 observed versus ≤2 predicted for Kumamoto, and 116 observed versus ≤7 predicted for Ridgecrest (Figure 2). This means that every potential shadow in the observed data that is the same size as

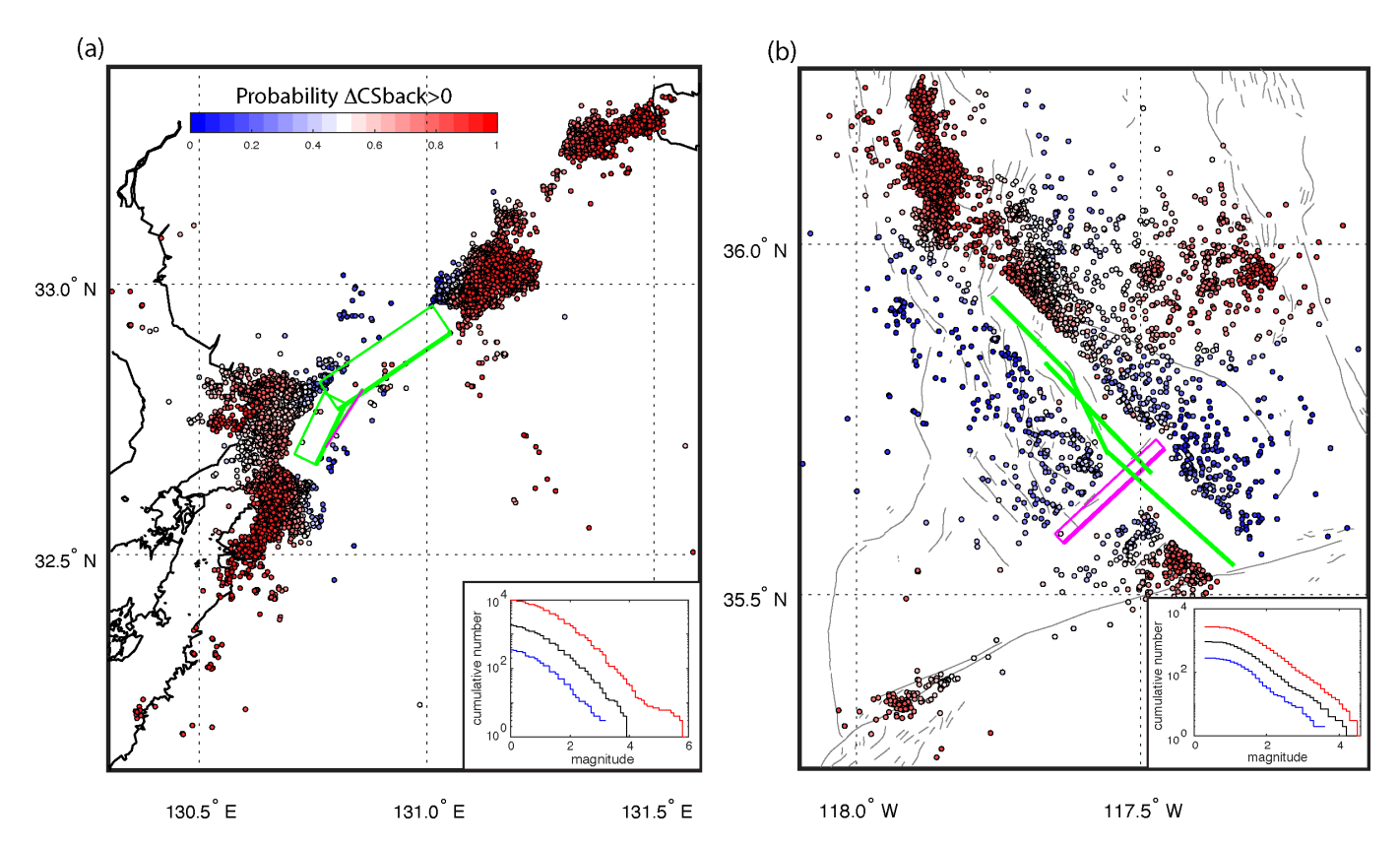


Figure 1 The probability of a positive Coulomb stress change for aftershocks \geq 4 km from the mainshock rupture during the first 2 weeks following the 2016 $\rm M_w$ 7.0 Kumamoto, Japan, and 2019 $\rm M_w$ 7.1 Ridgecrest, California, earthquakes. The Coulomb stress change, $\Delta CS_{\rm back}$, is projected on receiver faults representing the predominant active background faults. The probability of a positive Coulomb stress change, $P(\Delta CS_{\rm back}>0)$, is defined as the fraction of 2000 realizations of the stress change calculation in which the calculated $\Delta CS_{\rm back}$ is positive. (a) Map view of the Kumamoto sequence, earthquake locations from Japan Meteorological Agency (2024). Surface projection of mainshock fault from Asano and Iwata (2016) shown in green and foreshock in magenta, single line indicates vertical fault. (b) Map view of the Ridgecrest sequence, earthquake locations from SCSN catalog (California Institute of Technology and United States Geological Survey Pasadena, 1926). Surface projection of mainshock fault from Liu et al. (2019) shown in green and foreshock in magenta, single line indicates vertical fault. Insets show magnitude-frequency distributions: aftershocks in stress increase regions, $P(\Delta CS_{\rm back}>0)>2/3$, are shown in red, aftershocks in shadows, $P(\Delta CS_{\rm back}>0)<1/3$, are shown in blue, and all others in black.

the modeled stress shadows, and is coherent on a $\sim\!5$ km length scale, has more aftershocks than forecast by the CRS model. This supports the conclusion that the $\sim\!300$ observed aftershocks in the stress shadows are significantly more than predicted by the CRS model.

3.2 Testing Hypothesis 2: Unusual Receiver Faults

Another proposed explanation for aftershocks in stress shadows is that they occur on faults with very different orientations from the predominant fault orientations used as receiver faults, and that these unusual fault orientations experience increased rather than decreased Coulomb stress. This change in active planes could occur either with or without an observable rotation of the stress field. The CRS model predicts that in a region where a few faults experience a stress increase and most faults experience a stress decrease, there will be a rate increase followed by a rate decrease once the faults with a stress increase have failed (Marsan, 2006; Toda et al., 2012). This has been observed in some studies (Toda and Stein, 2002; Ma et al., 2005; Marsan and Nalbant, 2005;

Meng and Peng, 2014). Including receiver fault variability also improves the CRS model in testing (Mancini et al., 2019, 2020).

This hypothesis predicts that the focal mechanisms of aftershocks in the stress shadows are different from the local predominant fault orientation and have a positive ΔCS projected on their fault planes. There is some evidence for triggering on unusual planes from a global study that shows a shift in focal mechanism style between pre-mainshock earthquakes and aftershocks for some mainshocks (Mallman and Parsons, 2008). Segou and Parsons (2020) showed that for the 2010 M7.2 El Mayor-Cucapah aftershock sequence, there are large mean rotations between the optimally oriented planes and the set of planes receiving a positive Coulomb stress, suggesting that numerous unusual planes could be consistent with Coulomb stress triggering. Toda and Stein (2022) identify normal faulting in the hanging wall of the 2011 M9 Tohoku subduction earthquake as aftershocks on unusual planes, although it appears that normal faulting was active in these locations prior to the 2011 earthquake (Imanishi et al., 2012).

We test these predictions for the Ridgecrest and Ku-

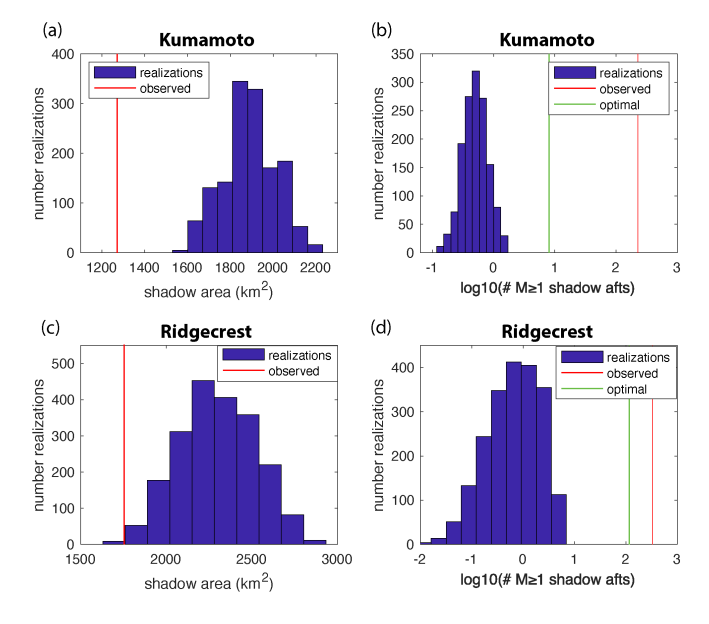


Figure 2 Comparison of the observed stress shadow size and number of shadow aftershocks with predictions from 2000 realizations of the Coulomb Rate and State (CRS) model. (a) The distribution of modeled stress shadow sizes for Kumamoto (blue histogram), compared to the observed size of the stress shadow (vertical red line). (b) The number of shadow aftershocks for Kumamoto predicted by the CRS model realizations (blue histogram), compared to the observed number of shadow aftershocks (vertical red line). Green vertical line shows the value for an optimal stress shadow: a collection of grid points the median size of the modeled shadows that has the minimum number of aftershocks. (c) The distribution of modeled stress shadow sizes for Ridgecrest, compared to the observed size of the stress shadow. (d) The number of shadow aftershocks for Ridgecrest predicted by the CRS model realizations, compared to the observed number and that of an optimal stress shadow.

mamoto aftershocks. We first investigate whether the focal mechanisms of the aftershocks in the stress shadows are unusual compared to the background mechanisms. The shadow aftershocks, $P(\Delta CS_{\text{back}} > 0)$ < 1/3, exhibit mechanisms that are more variable than the background earthquakes (Figure 3). Both sequences exhibit a trans-tensional background stress, and the focal mechanisms of the background earthquakes and the aftershocks in the stress increase regions reflect this with clustered sub-horizontal T-axes aligned with the extension direction, and an overlapping band of P- and B-axes. The focal mechanisms of the shadow aftershocks, in contrast, exhibit highly scattered P-, T-, and B-axes, with sub-horizontal to steeply plunging T-axes with a wide range of azimuths. That the focal mechanisms in the shadows are more scattered and less consistent with the background mechanisms supports the hypothesis that these events are occurring on unusual planes.

We next test whether these unusual planes experienced a positive static Coulomb stress change. We compute the earthquake-specific stress change, $\Delta CS_{\rm eq}$, using the locations and both focal mechanism nodal planes of the aftershocks as receivers (Fig-

ure 4). For both sequences, we find that a substantial fraction (30–50%) of the shadow aftershocks, defined as $P(\Delta CS_{\rm back}>0)<1/3$, also likely have a stress decrease on their focal mechanism nodal planes, $P(\Delta CS_{\rm eq}>0)<1/3$. Only a small fraction (5–15%) are likely to have a stress increase on the focal mechanism nodal planes, $P(\Delta CS_{\rm eq}>0)>2/3$. While there are some relatively large uncertainties in the individual event focal mechanisms (up to 45°), the lower-quality mechanisms are not disproportionately either consistent or inconsistent with a Coulomb stress increase.

This means that most of the shadow aftershocks can't be explained by positive Coulomb stress change either on the representative background faults or on the observed fault planes of the individual events. While the mechanisms of the shadow aftershocks do show fault plane variability, these unusual planes have not generally experienced a positive Coulomb stress change, inconsistent with the hypothesis of Coulomb stress triggering on unusual planes.

The stress shadow regions north of the Kumamoto mainshock exhibit background fault orientations that are a mix of mainshock-parallel strike-slip and East-West striking normal faults (Figure 5a). The fault planes of the individual event focal mechanisms also show a mix of strike-slip and normal faulting, with strike-slip planes generally subparallel to the mainshock, while the normal faults vary widely in strike. South of the Kumamoto mainshock, the shadow regions show background fault orientations that are predominately strikeslip planes subparallel to the southern part of the mainshock rupture. The individual event focal mechanisms show a wider range of strike-slip and normal faulting orientations. For the Ridgecrest earthquake (Figure 5b), the background faults in the shadow regions are almost entirely strike-slip on planes subparallel to the mainshock. The individual event focal mechanisms show a wide variety of strike-slip, normal, and even reverse fault orientations.

We also find a small population of events that occur in regions with positive stress changes on the background faults, but which have low probability of a positive stress change on the actual fault planes of the earthquakes (Figure 4). In both sequences (Figure 5), these events mostly occur within the densest aftershock clusters north of the northern end of the mainshock rupture. These events mostly exhibit normal-faulting or oblique-normal focal mechanisms, mostly accommodating extension in the direction towards the mainshock.

3.3 Testing Hypothesis 3: Alternative Frictional Properties

We next consider whether the faults that produce the shadow aftershocks may have different frictional properties, specifically whether they may be triggered primarily by shear or normal stress changes, rather than Coulomb stress change. Parsons et al. (1999) found that the seismicity on different faults can be more sensitive to either shear stress changes or normal stress changes. Laboratory observations indicate the importance of di-

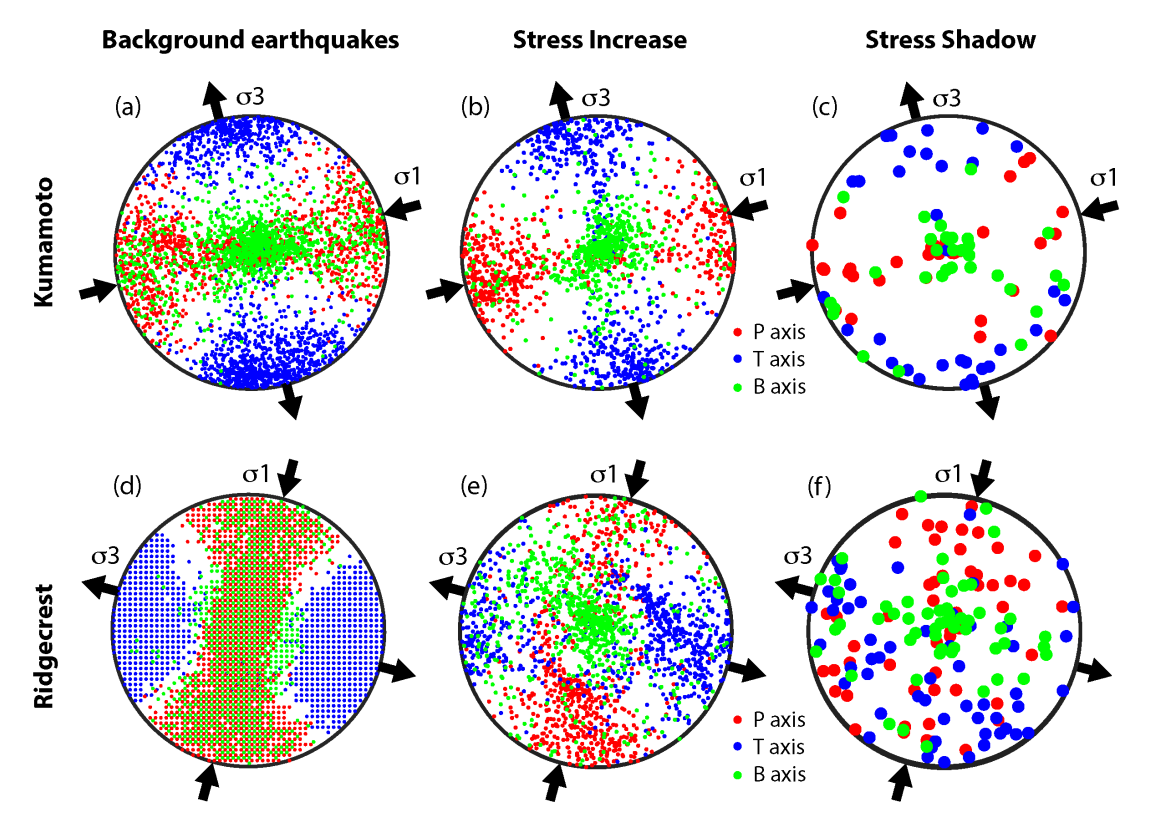


Figure 3 The distribution of P-, T-, and B-axes of aftershocks compared with background earthquakes. Focal mechanism from Uchide (2020) and Cheng et al. (2023) catalogs. (a) Axes of 1280 Kumamoto background earthquakes, 2005–2016, within 2 fault lengths of the mainshock (\sim 85 km). (b) Axes of 868 Kumamoto aftershocks in stress increase regions, $P(\Delta CS_{\rm back} > 0) > 2/3$. (c) Axes of 32 Kumamoto aftershocks in shadows, $P(\Delta CS_{\rm back} > 0) < 1/3$, shown with larger circles because of fewer events. (d) Axes of 17 609 Ridgecrest background earthquakes, 1981–2019, within 2 fault lengths of the mainshock (\sim 100 km) rasterized in order to represent a large number of events. (e) Axes of 786 Ridgecrest aftershocks in stress increase regions, $P(\Delta CS_{\rm back} > 0) > 2/3$. (f) Axes of 54 Ridgecrest aftershocks in shadows, $P(\Delta CS_{\rm back} > 0) < 1/3$, shown with larger circles because of fewer events. The arrows on the outside of the stereonets show the approximate orientations of the maximum (σ 1) and minimum (σ 3) principal stresses from inversion of background earthquake mechanisms (Michael, 1984).

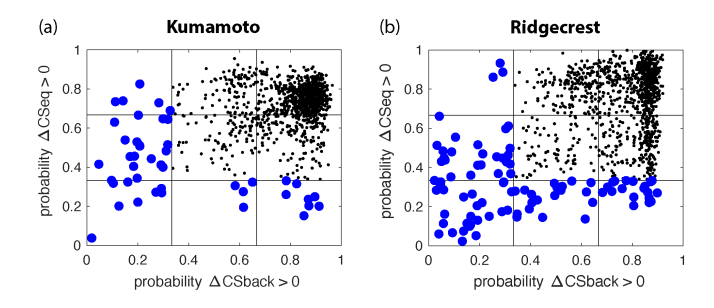


Figure 4 The probability of a positive Coulomb stress change using the background events as receiver planes, $P(\Delta C S_{\rm back} > 0)$, versus the probability using the individual event focal mechanisms as receiver planes, $P(\Delta C S_{\rm eq} > 0)$. Each point is an aftershock with an available focal mechanism. Aftershocks that are likely in a shadow by either measure are shown in with larger blue circles, and are shown in more detail in Figure 5 (a) Kumamoto aftershocks from the Uchide (2020) focal mechanism catalog (44 in shadow, 1042 not in shadow). (b) Ridgecrest aftershocks from the Cheng et al. (2023) focal mechanism catalog (94 in shadow, 1009 not in shadow).

latancy in rock failure (Beeler, 2007), suggesting that tensional normal or isotropic stress changes may play an important role in aftershock occurrence. Additionally, a tensional isotropic stress change will initially decrease the pore pressure, followed by a pore pressure increase as the pore pressure equilibrates, which may trigger aftershocks (e.g., Beroza and Zanzerkia, 2024).

We compute the probability of positive shear stress or normal stress (tension positive) change on the background faults, $P(\Delta \tau_{\rm back} > 0)$ and $P(\Delta \sigma_{\rm back} > 0)$, and on the individual event focal mechanism planes, $P(\Delta \tau_{\rm eq} > 0)$ and $P(\Delta \sigma_{\rm eq} > 0)$. We also compute the probability of a positive (tensional) isotropic stress change, $P(\Delta \sigma_{\rm kk} > 0)$, which is independent of the receiver fault orientation. We use the same suites of realizations of the stress change calculations as used to compute $\Delta CS_{\rm back}$ and $\Delta CS_{\rm eq}$.

For most shadow aftershocks (60–95%), there is a low probability (<1/3) of a positive shear or normal stress change, projected on the background faults, or of a positive isotropic stress change (Figure 6). For the earthquake-specific stress change, however, a considerable fraction of the shadow aftershocks (27–47%) have a high probability (>2/3) of a positive shear stress change on the nodal planes of the individual event focal mechanisms (Figure 7). This suggests that if static stress changes are the deciding factor, then these shadow aftershocks may be occurring on faults with low effective coefficients of friction (Equation 1). This could be due to

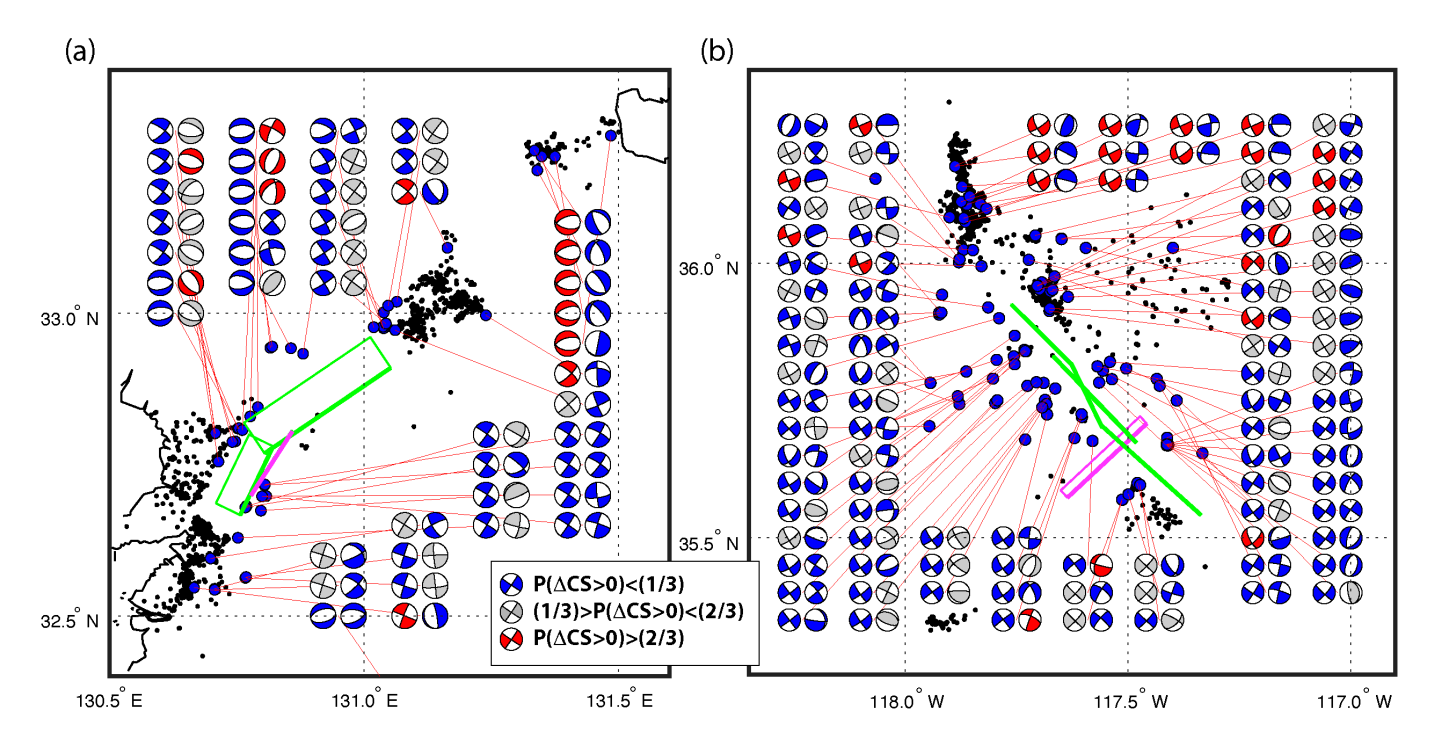


Figure 5 Map of focal mechanisms of aftershocks that are likely in a stress shadow. These events have a negative Coulomb stress change either on the representative background faults or on the focal mechanism nodal planes of the individual events (events in blue in Figure 4). Each aftershock is shown with two focal mechanisms: (left) the representative background mechanism, and (right) the individual event focal mechanism. Each mechanism is shaded corresponding to its probability of having a positive Coulomb stress change, $P(\Delta CS>0)$. (a) Kumamoto sequence, mainshock fault from Asano and Iwata (2016) shown in green and foreshock in magenta. Individual event focal mechanisms from Uchide (2020). (b) Ridgecrest sequence, mainshock fault from Liu et al. (2019) shown in green and foreshock in magenta. Individual event focal mechanisms from Cheng et al. (2023).

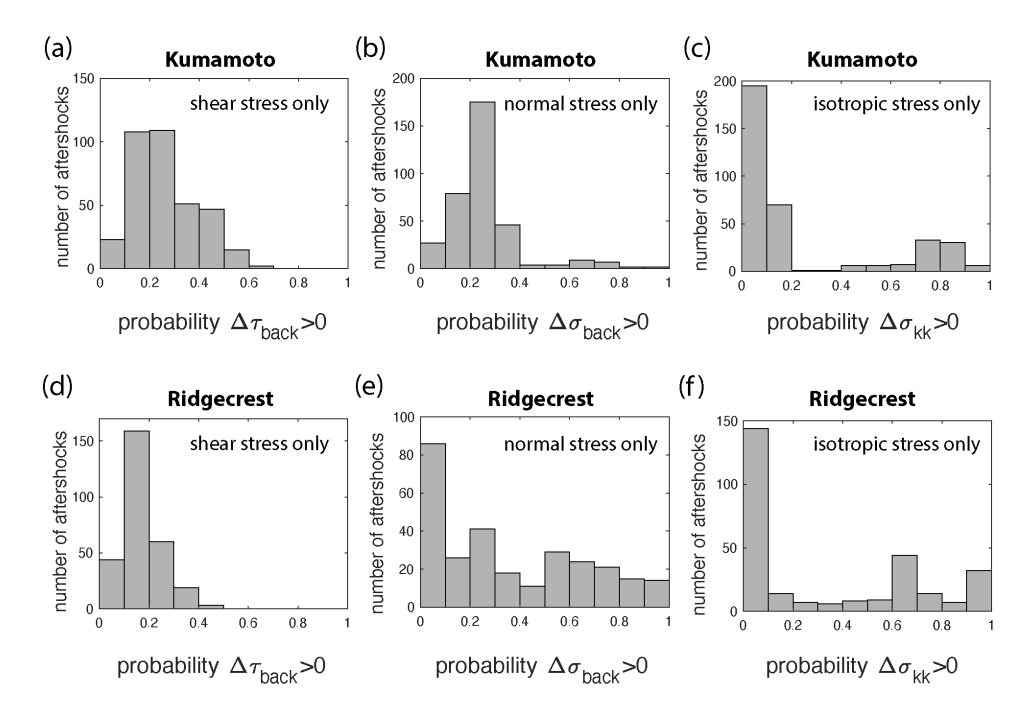


Figure 6 Probability of increase of individual stress components, for shadow aftershocks. Probability of an increase in shear stress ($\Delta \tau_{\rm back}$) or normal stress ($\Delta \sigma_{\rm back}$, tension positive) on representative background faults, and probability of a positive (tensional) isotropic stress change ($\Delta \sigma_{\rm kk}$). (a–c) Kumamoto, shown for the 355 earthquakes from Japan Meteorological Agency (2024) catalog that are defined as in the stress shadow, $P(\Delta CS_{\rm back}>0)<1/3$. (d–f) Ridgecrest, shown for the 285 earthquakes from SCSN catalog (California Institute of Technology and United States Geological Survey Pasadena, 1926) that are defined as in the stress shadow.

low intrinsic friction or changes in fluid pressure that

largely counteract the normal stress changes. The Ku-

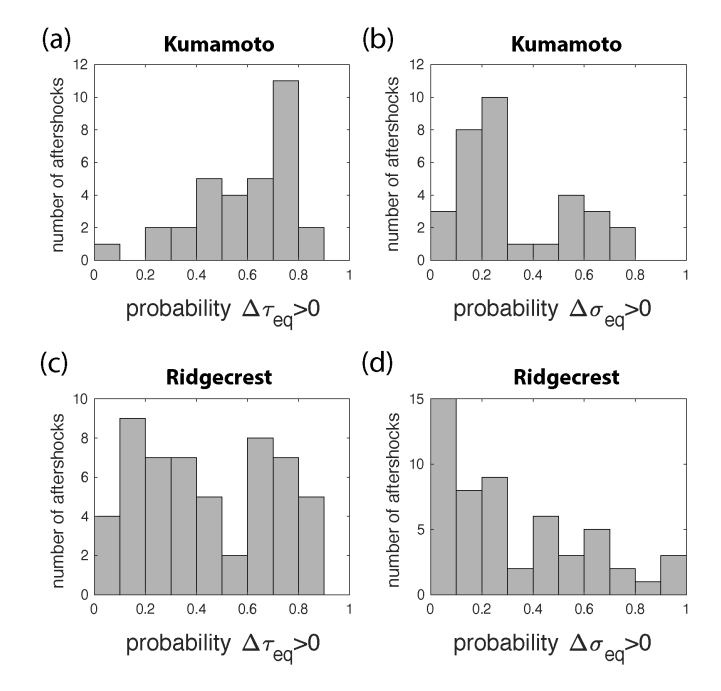


Figure 7 Probability of increase of individual stress components, for shadow aftershocks. Probability of an increase in shear stress $(\Delta\tau_{\rm eq})$ and normal stress $(\Delta\sigma_{\rm eq})$ on the nodal planes of individual earthquake focal mechanisms. (a–b) Kumamoto, 32 earthquakes in the Uchide (2020) focal mechanism catalog that are identified as in the stress shadow, $P(\Delta CS_{\rm back} > 0) < 1/3$. (c–d) Ridgecrest, 54 earthquakes in the Cheng et al. (2023) focal mechanism catalog that are identified as in the stress shadow.

mamoto aftershocks exhibiting $P(\Delta \tau_{\rm eq}>0)$ are disproportionally more shallow events, suggesting that low effective friction may be related to the lower confining stress. There is no dependence with depth for Ridgecrest, however.

3.4 Testing Hypothesis 4: Secondary Triggering

Many aftershocks are secondary, meaning that they are not triggered directly by the mainshock, but by previous aftershocks (e.g., Felzer et al., 2003). Aftershocks may also be indirectly triggered by afterslip following the mainshock (e.g., Cattania et al., 2015), and a connection between afterslip and aftershocks is suggested by the similar temporal decay (e.g., Perfettini and Avouac, 2004). However, the secondary stress changes are often too small to counteract the negative stress changes from the mainshock and can themselves be negative (e.g., Segou and Parsons, 2014; Meier et al., 2014).

We investigate secondary triggering from prior aftershocks using 1000 realizations of Epidemic-Type Aftershock Sequence (ETAS) stochastic declustering (Zhuang et al., 2002) to identify the likely "parent" earthquake of each after-shock (Table 1). The ETAS parameters were fit to each catalog. The ETAS model for the rate of aftershocks of magnitude $\geq M$ at time t is:

$$\lambda(t, M) = k \sum_{\{i: t_i < t\}} e^{a(M_i - M)} (t - t_i + c)^{-p}$$
 (5)

where t_i and M_i are the time and magnitude of prior earthquake i. For the Kumamoto sequence, a=0.99, p=1.11, c=0.0051 days, and k=0.0026, and for Ridgecrest a=0.99, p=1.12, c=0.00063 days, and k=0.0032. Inputs to the declustering include the mainshock and M≥6 foreshocks, as well as all aftershocks including those <4 km from the mainshock fault. Over the multiple realizations, we find that $\sim 60-70\%$ of the shadow aftershocks are identified as triggered by the mainshock or a foreshock. While secondary triggering can explain $\sim 30-40\%$ of the shadow aftershocks, the majority appear to be directly triggered by the mainshock. Typically, $\sim 50\%$ of aftershocks are secondary (Felzer et al., 2003), so shadow aftershocks are slightly less likely than average to be secondary.

	Percent of shadow after- shocks (distance ≥4 km) with parent type	
Parent event type	Ridgecrest	Kumamoto
	sequence	sequence
Mainshock or foreshock	71.4±1.5%	58.2±2.3%
Shadow aftershock	11.6±1.0%	11.1±1.4%
Stress increase aftershock	1.9±0.5%	10.4±1.5%
Ambiguous aftershock	3.2±0.6%	7.1±1.2%
Near-fault aftershock	11.9±1.2%	13.1±1.7%

Table 1 The type of parent earthquake for each aftershock in the stress shadow, ≥ 4 km from the mainshock. The parent is either the mainshock or a foreshock, another aftershock ≥ 4 km from the mainshock that is categorized as being in a shadow, a stress increase region, or with ambiguous stress change, or a near-fault aftershock <4 km from the mainshock. The mean and standard deviation of the percent of shadow aftershocks with each type of parent is shown, over 1000 realizations of stochastic declustering.

We investigate secondary triggering from afterslip by modeling the static stress changes from the afterslip models of Liu et al. (2024) for Kumamoto, and Yue et al. (2021) for Ridgecrest. We compute Coulomb stress changes following the same modeling steps as for the coseismic stress changes, except that we use a single afterslip dislocation model, along with a range of receiver fault orientations and coefficients of friction. With background faults as receivers (Figure 8a,c), the majority of the shadow aftershocks have a low (<1/3) probability of a positive stress change from afterslip. For Kumamoto, this also holds true for the earthquakespecific stress changes (Figure 8b). However, for Ridgecrest, 24% of the shadow aftershocks have a high (>2/3) probability of a positive stress change from afterslip on the focal mechanism nodal planes (Figure 8d). While afterslip does not appear to be a general triggering mechanism for the majority of the shadow aftershocks, it may have had some influence on the Ridgecrest sequence.

3.5 Near-fault Aftershocks

We did not use aftershocks within 4km of the mainshock fault plane when testing the four hypotheses. This is due to the difficulty of modeling the stress

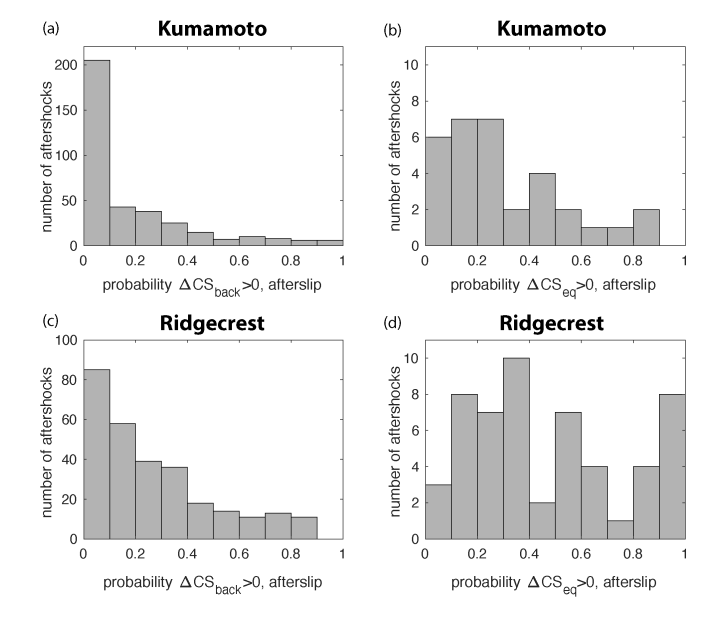


Figure 8 The probability of a positive Coulomb stress change from afterslip, for aftershocks in the stress shadow $(P(\Delta CS_{\mathrm{back}} > 0) < 1/3)$. The background events or the individual event focal mechanisms are used as receiver planes. (a) Background $P(\Delta CS_{\mathrm{back}} > 0)$ for Kumamoto afterslip, earthquakes from Japan Meteorological Agency (2024) catalog. (b) Event-specific $P(\Delta CS_{\mathrm{eq}} > 0)$ for Kumamoto afterslip, earthquakes from Uchide (2020) focal mechanism catalog. (c) Background $P(\Delta CS_{\mathrm{back}} > 0)$ for Ridgecrest afterslip, earthquakes from SCSN catalog (California Institute of Technology and United States Geological Survey Pasadena, 1926). (d) Event-specific $P(\Delta CS_{\mathrm{eq}} > 0)$ for Ridgecrest afterslip, earthquakes from the Cheng et al. (2023) focal mechanism catalog.

changes this close to the mainshock rupture, given that the resolution of the slip models is usually on the order of a few km. However, many aftershocks occur along or very near the mainshock rupture (including 37% of the Kumamoto and 72% of the Ridgecrest aftershocks), and these events often appear to be in a static Coulomb stress shadow. This is because stress changes on the local predominant fault orientations are often negative close to the mainshock, as the mainshock slip relieves shear stress on the mainshock fault plane and subparallel faults.

There are two models that reconcile these near-fault aftershocks with the static Coulomb stress change triggering model. The first model is that the aftershocks do not occur on faults similar to the mainshock, but instead on optimally oriented faults in the total stress field. Near to the mainshock, the optimally oriented faults are usually highly rotated from the predominant fault orientation (e.g., King et al., 1994). The second model is that spatially variable mainshock stress drop, on scales too small to be captured by mainshock slip models, leads to stress heterogeneity and patches of stress increase on mainshock-parallel planes (Marsan, 2006; Helmstetter and Shaw, 2006).

Both models should apply to aftershocks within 4 km of the mainshock rupture. Marsan (2006) used a fractal slip model, with dimension based on observed slip

distributions, and found that it can load stress on mainshock-parallel planes at distances up to at least 1 km but not as far as 5 km. Helmstetter and Shaw (2006) computed the range of this effect to be 10% of the mainshock fault length, which is \sim 40 km for a M7 mainshock (Wells and Coppersmith, 1994). A distance of \sim 4 km is also consistent with the nearfield fault rotations seen in modeling of optimally oriented planes (e.g., King et al., 1994).

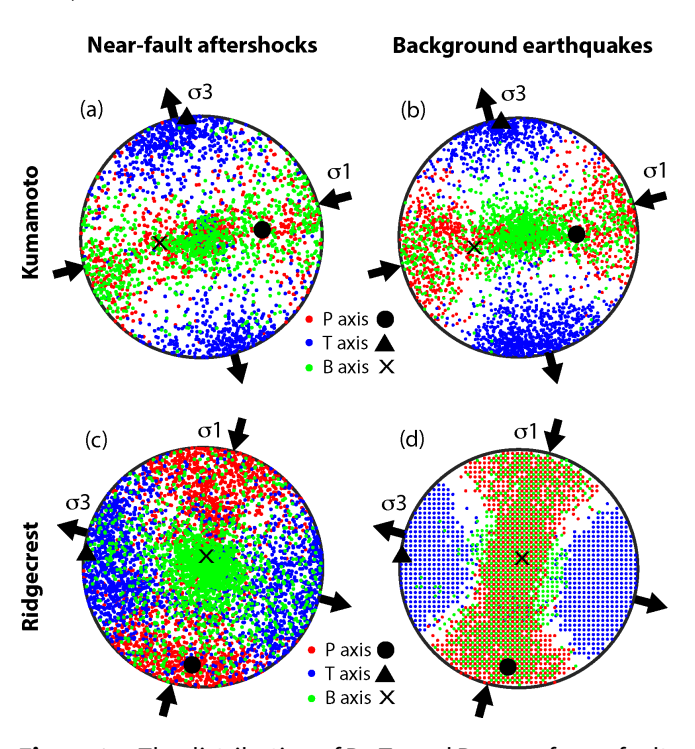


Figure 9 The distribution of P-, T-, and B-axes of near-fault aftershocks (within 4 km of the mainshock) compared with the mainshock and background earthquakes. Focal mechanism from the Uchide (2020) and Cheng et al. (2023) catalogs. (a) Axes of 1044 Kumamoto near-fault aftershocks. (b) Axes of 1280 Kumamoto background earthquakes, 2005-2016, within 2 fault lengths of the mainshock (\sim 85 km). (c) Axes of 2139 Ridgecrest near-fault aftershocks. (d) Axes of 17 609 Ridgecrest background earthquakes, 1981-2019, within 2 fault lengths of the mainshock (\sim 100 km), rasterized in order to represent a large number of events. The black circles, triangles and X's represent the P-, T-, and Baxes of the mainshock, respectively. The arrows on the outside of the stereonets show the approximate orientations of the maximum (σ 1) and minimum (σ 3) principal stresses from inversion of background earthquake mechanisms.

These two models have different predictions for the near-fault aftershock focal mechanisms: the optimally oriented plane model predicts that they will be very different from the mainshock mechanism, while the variable stress drop model allows them to be similar. We use the focal mechanism catalogs of Uchide (2020) and Cheng et al. (2023) to test the predictions of these two models. For both sequences, we find that the focal mechanisms of the near-fault aftershocks have similar orientation as the mainshock and the background earthquakes, and are consistent with being driven by the background stress (Figure 9). This is inconsistent with the prediction of the optimally oriented plane

model that the activated faults are highly rotated from the mainshock orientation, and consistent with the variable stress drop model.

4 Discussion

4.1 Static Stress Changes

Close to the mainshock (<4 km distance), we are unable to determine if any specific aftershock is consistent with static Coulomb stress triggering, due to the lack of resolution of the slip models. We show that these nearfault aftershocks typically occur on fault planes similar to those of the mainshock and the background events, inconsistent with the hypothesis that these events occur on substantially rotated optimally oriented planes (e.g., King et al., 1994). Within 4 km of the fault, unmodeled small-scale mainshock slip heterogeneity can lead to stress heterogeneity including positive Coulomb stress change on some faults subparallel to the mainshock (Marsan, 2006; Helmstetter and Shaw, 2006). Therefore, the near-fault aftershocks as a whole are plausibly consistent with static Coulomb stress triggering.

For events >4 km from the mainshock, we find 355 (Kumamoto) and 285 (Ridgecrest) catalog aftershocks with low probability (<1/3) of having experienced a static Coulomb stress increase, given a suite of realizations of the stress change modeling with a range of mainshock models and receiver faults. Declustering indicates that \sim 60-70% of these events were directly triggered by the mainshock, implying ~200 direct aftershocks in each sequence that likely experienced a Coulomb stress decrease. While any one of these events has some probability of having experienced a positive stress change, there is a very low probability that all of them did. We also find that the number of aftershocks in the stress shadow, including an optimized shadow with a minimum number of events, is substantially larger than predicted by the CRS model in any of the realizations of the calculated Coulomb stress change. This implies that many aftershocks do occur in stress shadows, even when considering the impacts of mainshock source model uncertainty and the uncertainty of the aftershock fault plane. Note that both the mainshock slip distributions and the receiver fault orientations are likely better constrained for the recent Kumamoto and Ridgecrest earthquakes than for the older Landers earthquake studied by Hainzl et al. (2009).

We test several hypotheses that attempt to reconcile the shadow aftershocks with the static stress change triggering model (Table 2). None of the individual hypotheses explain even half of the shadow aftershocks, and only 50–56% of the shadow aftershocks with available focal mechanisms are explained by at least one of the hypotheses. One of the most common hypotheses is that the shadow aftershocks occur on faults of unusual orientations that receive a positive static stress change, despite the negative static stress change on the surrounding faults of the predominant orientation (e.g., Toda and Stein, 2002). We do find that many of the shadow aftershocks occur on fault planes of unusual orientation. However, only 5–15% have a high proba-

bility (>2/3) of a static Coulomb stress increase while 30–50% have a low probability (<1/3) of a stress increase.

The occurrence of the shadow aftershocks on unusual fault plane orientations may hold some clues to the physical mechanisms behind their triggering. While the background planes in the stress shadows do not generally receive a stress increase from afterslip, 24% of the Ridgecrest shadow aftershocks have a high probability (>2/3) of a stress increase on the focal mechanism nodal planes. The focal mechanism nodal planes also have a higher rate of shear stress increase compared to the background fault planes, with 27-47% of the shadow aftershocks having a high (>2/3) probability of shear stress increase. This suggests that some shadow aftershocks occur on faults with low effective coefficient of friction (Equation 1), due to either low intrinsic friction or changes in fluid pressure that largely counteract the normal stress changes. Low frictional strength could also explain why failure can occur on faults that are poorly aligned with the background stress, and therefore have low total resolved shear stress. However, these explanations only apply to a fraction of the shadow aftershocks.

4.2 Stress Concentrations Due to Material Heterogeneity

The modeled Coulomb stress changes used in these tests are approximations of the true Coulomb stress changes, and specifically do not capture effects of material heterogeneity. Material heterogeneity has been linked to stress variability (e.g., Martínez-Garzón et al., 2025). It is unclear, however, how much effect unmodeled structure may have on the calculated Coulomb stress changes. Sharma et al. (2020) found that using a layered half-space versus a homogeneous half-space does not substantially change the Coulomb stress calculations. Localized stress change heterogeneity may also occur where stress change is focused or amplified due to fault discontinuities, damage zones, or asperities. These types of small-scale spatial features are difficult to impossible to observe at depth in general and the information is not available for either the Kumamoto or Ridgecrest earthquake settings. Therefore, it was not possible to include those details in our Coulomb stress calculations. This means it is possible that the shadow aftershocks are responding to local increases in Coulomb stress change that cannot be captured by the type of Coulomb stress change modeling that is currently feasible.

4.3 Postseismic Relaxation Processes

The stress in the crust continues to change after the coseismic stress changes, due to post-seismic processes including viscoelastic relaxation and poroelastic rebound. These processes have been shown to influence the occurrence of earthquakes over years to decades (e.g., Beroza and Zanzerkia, 2024; Pollitz and Cattania, 2017). The timescales of these relaxation processes are generally on the order of years. For example, the viscosity in the Kumamoto area is estimated to be $\eta=$

Hypothesis 1: Aftershocks appear to be in shadows because of inaccuracy in the inputs to the stress change calculations (e.g., mainshock slip model, receiver faults, fault friction).	Inconsistent, 285–355 aftershocks (distance >4 km) consistently in shadows over multiple modeling choices.	
Hypothesis 2: Aftershocks in the shadows occur on faults with different orientations than		
the model receiver faults, and these unexpected fault orientations experience increased	Explains 5–15% of shadow aftershocks.	
Coulomb stress.		
Hypothesis 3: Aftershocks in the shadows have different friction properties, are triggered	change. Explains 27–47% of snadow aftersnocks.	
by shear or normal stress changes, not by Coulomb stress change.		
Hypothesis 4: Aftershocks in the shadows are secondary aftershocks triggered by prior af-	Explains 29–42% of shadow aftershocks.	
tershocks or afterslip.		
All Hypotheses: Aftershocks in the shadows, with available focal mechanism, explained by	Explains 50% (Kumamoto) to 56%	
at least one of the hypotheses.	(Ridgecrest) of shadow aftershocks.	

Table 2 Summary of the tested hypotheses, with both a brief description of each hypothesis, and an estimate of how many shadow aftershocks are explained or unexplained by that hypothesis.

 $2\times 10^{19}\,\mathrm{Pa}\cdot\mathrm{s}$ (Liu et al., 2024), so if the elastic modulus is $E=30\,\mathrm{GPa}$, the characteristic relaxation time is $\eta/E=21\,\mathrm{years}$. Poroelastic rebound occurs as the pore pressure equilibrates from the undrained to drained state (e.g., Beroza and Zanzerkia, 2024). The coseismic isotropic stress, and hence the pore pressure change, at $\geq 4\,\mathrm{km}$ from the mainshock varies spatially on length scales of >5 km. For a diffusivity of $D=0.1\,\mathrm{m}^2/\mathrm{s}$, and a length scale of $L=5\,\mathrm{km}$, the diffusion time would be on the order of $L^2/D=8\,\mathrm{years}$. Closer to the mainshock, poroelastic rebound may play a role in aftershock triggering over the first few weeks, as appears to be the case for the 2025 M7.1 Tingri, Tibet, earthquake (Yue et al., 2025).

Many of the Ridgecrest shadow aftershocks on the northwest side of the mainshock (Figure 1b) are in an area of fault-normal postseismic surface displacement, inferred from GNSS and InSAR, which was interpreted by Brooks et al. (2020) to indicate poroelastic effects. The largest GNSS displacements occur within the first few weeks following the mainshock, so are active on the time frame of the observed aftershocks in the stress shadows. Extension in this region could reduce normal stress on mainshock-parallel faults and promote aftershocks. However, shadow aftershocks also occur on the east side of the fault where fault-parallel postseismic surface displacement indicates afterslip with no substantial component of extension.

The Coso geothermal field, which experiences pore pressure changes from geothermal energy production, falls within the Ridgecrest stress increase region. However, the Ridgecrest earthquake triggered few aftershocks at Coso, likely because decades of net fluid production and decreasing temperature destressed the faults (Im et al., 2021). While the Coso area is not in a stress shadow, it does illustrate that the pore pressure and temperature history of a location may have a significant impact on aftershock occurrence.

In addition to poroelastic rebound, fluid pressure may be affected by an influx of fluids from below the seismogenic zone. For the Kumamoto earthquake, Nakagomi et al. (2021) inferred large increases in pore pressure from below in the southwestern part of the aftershock zone (Figure 1a). They also find that many aftershocks occur in regions where they infer high pore

pressure prior to the sequence, including locations in static Coulomb stress shadows. However, the highest overpressures are also concentrated in the southwestern part of the aftershock zone. Increased earthquake rates observed in other stress shadow locations are not as well explained by this model.

4.4 Dynamic Stress Changes

Dynamic stress triggering due to the passing seismic waves is a plausible alternative to the static Coulomb stress triggering model. The maximum dynamic Coulomb stresses are never negative (e.g., Kilb et al., 2000), so the aftershocks in the static stress shadows could be dynamically triggered. Evidence for the importance of dynamic triggering in the aftershock zone (within \sim 2 fault lengths of the mainshock) comes from multiple types of observations. Asymmetry is observed in some aftershock spatial distributions that matches the directivity of the mainshock, with more aftershocks occurring where the dynamic stress changes are highest (Kilb et al., 2000; Gomberg et al., 2003). Pollitz and Johnston (2006) compared the aftershocks of earthquakes versus nearly-colocated slow-slip events and found that the earthquakes produced many more aftershocks, implying that the dynamic seismic waves contributed substantially to aftershock triggering. van der Elst and Brodsky (2010) projected far-field dynamic triggering rates into the aftershock zone and found that a substantial fraction of the aftershocks are likely dynamically triggered. Hardebeck and Harris (2022) found that the rate of aftershocks in the stress shadows decays with distance and time from the mainshock as expected from dynamic triggering. Dynamic triggering must include a mechanism for delayed triggering to explain how aftershocks continue after the seismic waves have passed. Proposed mechanisms include rate and state friction (e.g., van der Elst and Savage, 2015), changes in frictional properties (e.g., Parsons, 2005; Johnson et al., 2008; Felzer, 2014), and permeability and pore pressure changes (e.g., Brodsky et al., 2003).

Both van der Elst and Brodsky (2010) and Hardebeck and Harris (2022) estimate that \sim 15–60% of aftershocks are dynamically triggered. Similarly, Parsons (2002) found that 39% of global aftershocks occur on faults

with a static stress decrease. A hybrid static-dynamic triggering model with 2/3 static and 1/3 dynamic stress triggering provides a good approximation of the aftershock spatial distribution (Hardebeck and Harris, 2022). A hybrid model can also explain observations of an initial seismicity rate increase due to dynamic stresses followed by a rate decrease due to a static stress decrease (e.g., Meng and Peng, 2014; Ma et al., 2005).

4.5 Continuing Background Earthquakes

While the CRS model predicts a substantial decrease in the rate of earthquakes in the stress shadows, continued background earthquakes are possible. Specifically, faults that were already near failure may produce earthquakes that are only slightly delayed. For example, Harris and Simpson (1998) show that the 1911 M6.6 Morgan Hill earthquake that occurred in the stress shadow of the 1906 San Francisco earthquake may have been such an event.

For the Kumamoto and Ridgecrest aftershock sequences, the rate of aftershocks in the shadows during the first 2 weeks is clearly above the background rate. There are over 100 M≥1.0 aftershocks in the shadows (Figure 1), for an average rate of >7 events/day. In contrast, the background rate in the stress shadow regions is on the order of \sim 1 M \geq 1.0 event/day for both regions, as computed from the Japan Meteorological Agency (2024) and SCSN (California Institute of Technology and United States Geological Survey Pasadena, 1926) catalogs. The expected earthquake rate decrease from the CRS model (Equation 2) can be computed for shadow regions 4-40 km from the mainshock fault, given values of ΔCS_{back} computed on a grid. We find that the overall expected decrease is \sim 2–3 orders of magnitude, to a rate of ~0.001–0.01 M≥1.0 event/day. Therefore, it is unlikely that many of the hundreds of shadow aftershocks were background events that were already near failure.

The CRS model can predict a rate increase in the stress shadows, if there is a distribution of active fault plane orientations in the shadows. Rate can increase if there are some faults of unusual orientations that experience a stress increase, in addition to the predominant faults which experience a stress decrease (e.g., Marsan, 2006; Toda and Stein, 2022). The rate increase in this model comes from triggering of aftershocks on the unusual fault planes with positive stress changes. However, we found in Section 3.2 that most of the aftershocks occurring in the shadows do not have a positive stress change on their focal mechanism nodal planes, so this model can't explain their occurrence.

5 Conclusions

We investigate multiple hypotheses for the occurrence of aftershocks in static Coulomb stress shadows following the 2016 $\rm M_w 7.0~Kumamoto$, Japan, and 2019 $\rm M_w 7.1~Ridgecrest$, California, earthquakes. In particular, we test hypotheses that attempt to reconcile these aftershocks with the static Coulomb stress triggering model, which predicts a substantial decrease in earthquake rate in the shadows. These hypotheses are: (1) the

shadow aftershocks appear to be in shadows because of inaccuracy in the stress change calculations, (2) they occur on faults of unusual orientation which experience increased Coulomb stress, (3) they occur on faults with different frictional properties, not modeled well by Coulomb stress, and (4) they are secondary aftershocks triggered by prior aftershocks or afterslip. None of these hypotheses explain the majority of the shadow aftershocks, and only ${\sim}50\%$ of shadow aftershocks are explained by at least one of the hypotheses.

We demonstrate that aftershocks do not fall within stress shadows just due to inaccuracy in the calculated static Coulomb stress change. For both sequences, we find hundreds of aftershocks with high probabilities of occurrence in a stress shadow across 2000 realizations of the stress change calculations with: varying mainshock slip models, including or not including foreshocks, multiple choices of the receiver fault, and multiple values of the effective coefficient of friction. We find that only 5-15% of shadow aftershocks with available focal mechanisms likely experienced a static Coulomb stress increase on their focal mechanism nodal planes. This is contrary to another common explanation of shadow aftershocks as occurring on faults with unusual orientations that experienced a Coulomb stress increase.

There is some evidence that the active faults in the shadows may be more sensitive to changes in shear stress than to changes in Coulomb stress. Some of the shadow aftershocks (27–47%) experienced a positive shear stress change on the nodal planes of the individual event focal mechanisms. This suggests that at least some of the shadow aftershocks may occur on faults with low effective coefficients of friction.

We further test whether the shadow aftershocks could be secondary events triggered by previous aftershocks or by afterslip. We find that the majority of the shadow aftershocks (58–71%) for both sequences are likely to have been triggered directly by the mainshock. About 24% of the Ridgecrest shadow aftershocks are consistent with triggering by afterslip, while only $\sim\!10\%$ of Kumamoto shadow aftershocks are consistent. So while most shadow aftershocks do not appear to be secondary, it is possible that afterslip may play a role in some cases.

We acknowledge that the modeled Coulomb stress changes in this study are approximations. They don't capture localized stress concentrations that may occur due to fault zone heterogeneity such as fault discontinuities, damage zones, or asperities. Therefore, it is possible that the shadow aftershocks are responding to local increases in Coulomb stress change that cannot be captured by the type of Coulomb stress change modeling presented here.

We consider some alternative models for triggering in the stress shadows, based on physical mechanisms other than static Coulomb stress change. Relaxation processes including viscoelastic relaxation and poroelastic rebound generally act on time scales that are too long to explain the immediate increase in seismicity in the stress shadows. For both the Ridgecrest and Kumamoto earthquakes, however, there are suggestions that pore fluid pressure changes may have played a role

in triggering (Brooks et al., 2020; Nakagomi et al., 2021). Delayed dynamic stress triggering due to the passing seismic waves is a plausible triggering mechanism, and a hybrid static-dynamic model provides a good approximation of the spatial and temporal occurrence of aftershocks (Hardebeck and Harris, 2022).

Acknowledgements

We thank Debi Kilb, Davide Zaccagnino, Fred Pollitz, Tom Parsons, and an anonymous reviewer for thorough reviews that helped improve the manuscript. Any use of trade, firm, or product names is for descriptive purposes only and does not imply endorsement by the U.S. Government.

Data and Code Availability

The JMA catalog (Japan Meteorological Agency, 2024) is available at https://www.data.jma.go.jp/svd/ eqev/data/bulletin/eqdoc_e.html (last accessed August 9, 2024). The SCSN catalog (California Institute of Technology and United States Geological Survey Pasadena, 1926) was accessed through the Southern California Earthquake Data Center (SCEDC, 2013) https://service.scedc.caltech.edu/eq-catalogs/date_ mag_loc.php (last accessed August 28, 2024). focal mechanism catalog of Uchide (2020) was downloaded from https://github.com/uchide/Uchide2020GJI (last accessed June 11, 2025). The focal mechanism catalog of Cheng et al. (2023) was downloaded from https://scedc.caltech.edu/data/alt-2022-cheng.html (last accessed June 11, 2025). The SRCMOD Earthquake Source Model Database (Mai and Thingbaijam, 2014) is available at http://equake-rc.info/srcmod/ (last accessed June 11, 2025). The Kubo et al. (2016) model was obtained from https://www.kyoshin.bosai.go.jp/ kyoshin/inversion/inversion_main_en.shtml (last cessed August 14, 2024). The Okada (1992) code to model dislocations in an elastic half-space is publicly available at https://www.bosai.go.jp/e/dc3d.html (last accessed June 11, 2025). All other data from the cited references.

Competing Interests

The authors have no competing interests.

References

- Asano, K. and Iwata, T. Source rupture processes of the foreshock and mainshock in the 2016 Kumamoto earthquake sequence estimated from the kinematic waveform inversion of strong motion data. *Earth, Planets and Space*, 68(1), Aug. 2016. doi: 10.1186/s40623-016-0519-9.
- Barnhart, W. D., Hayes, G. P., and Gold, R. D. The July 2019 Ridgecrest, California, Earthquake Sequence: Kinematics of Slip and Stressing in Cross-Fault Ruptures. *Geophysical Research Letters*, 46(21):11859–11867, Nov. 2019. doi: 10.1029/2019gl084741.
- Beeler, N. M. 13. Laboratory-Observed Faulting in Intrinsically and Apparently Weak Materials: Strength, Seismic Coupling, Dila-

- tancy, and Pore-Fluid Pressure, page 370–449. Columbia University Press, Dec. 2007. doi: 10.7312/dixo13866-013.
- Beroza, G. and Zanzerkia, E. E. An Unambiguous Signature of Pore Fluid Aftershock Triggering in the Landers Earthquake Sequence. *Annals of Geophysics*, 67(4):S432, Oct. 2024. doi: 10.4401/ag-9162.
- Brodsky, E. E., Roeloffs, E., Woodcock, D., Gall, I., and Manga, M. A mechanism for sustained groundwater pressure changes induced by distant earthquakes. *Journal of Geophysical Research: Solid Earth*, 108(B8), Aug. 2003. doi: 10.1029/2002jb002321.
- Brooks, B. A., Murray, J., Svarc, J., Phillips, E., Turner, R., Murray, M., Ericksen, T., Wang, K., Minson, S., Burgmann, R., Pollitz, F., Hudnut, K., Nevitt, J., Roeloffs, E., Hernandez, J., and Olson, B. Rapid Geodetic Observations of Spatiotemporally Varying Postseismic Deformation Following the Ridgecrest Earthquake Sequence: The U.S. Geological Survey Response. *Seismological Research Letters*, 91(4):2108–2123, May 2020. doi: 10.1785/02202000007.
- California Institute of Technology and United States Geological Survey Pasadena. Southern California Seismic Network, 1926. doi: 10.7914/SN/CI.
- Cattania, C., Hainzl, S., Wang, L., Enescu, B., and Roth, F. Aftershock triggering by postseismic stresses: A study based on Coulomb rate-and-state models. *Journal of Geophysical Research: Solid Earth*, 120(4):2388–2407, Apr. 2015. doi: 10.1002/2014jb011500.
- Cheng, Y., Hauksson, E., and Ben-Zion, Y. Refined Earthquake Focal Mechanism Catalog for Southern California Derived With Deep Learning Algorithms. *Journal of Geophysical Research: Solid Earth*, 128(2), Feb. 2023. doi: 10.1029/2022jb025975.
- DeVries, P. M. R., Viégas, F., Wattenberg, M., and Meade, B. J. Deep learning of aftershock patterns following large earthquakes. *Nature*, 560(7720):632–634, Aug. 2018. doi: 10.1038/s41586-018-0438-v.
- Dieterich, J. A constitutive law for rate of earthquake production and its application to earthquake clustering. *Journal of Geophysical Research: Solid Earth*, 99(B2):2601–2618, Feb. 1994. doi: 10.1029/93jb02581.
- Felzer, K., Abercrombie, R., and Ekström, G. Secondary Aftershocks and Their Importance for Aftershock Forecasting. *Bulletin of the Seismological Society of America*, 93(4):1433–1448, Aug. 2003. doi: 10.1785/0120020229.
- Felzer, K. R. Pulverization provides a mechanism for the nucleation of earthquakes at low stress on strong faults. *Frontiers in Earth Science*, 2, Aug. 2014. doi: 10.3389/feart.2014.00020.
- Felzer, K. R. and Brodsky, E. E. Testing the stress shadow hypothesis. *Journal of Geophysical Research: Solid Earth*, 110(B5), May 2005. doi: 10.1029/2004jb003277.
- Gomberg, J., Bodin, P., and Reasenberg, P. Observing Earthquakes Triggered in the Near Field by Dynamic Deformations. *Bulletin of the Seismological Society of America*, 93(1):118–138, Feb. 2003. doi: 10.1785/0120020075.
- Hainzl, S., Enescu, B., Cocco, M., Woessner, J., Catalli, F., Wang, R., and Roth, F. Aftershock modeling based on uncertain stress calculations. *Journal of Geophysical Research: Solid Earth*, 114(B5), May 2009. doi: 10.1029/2008jb006011.
- Hardebeck, J. and Shearer, P. A New Method for Determining First-Motion Focal Mechanisms. Bulletin of the Seismological Society of America, 92(6):2264–2276, Aug. 2002. doi: 10.1785/0120010200.
- Hardebeck, J. L. and Harris, R. A. Earthquakes in the Shadows: Why Aftershocks Occur at Surprising Locations. *The Seismic Record*, 2(3):207–216, July 2022. doi: 10.1785/0320220023.
- Harris, R. A. and Simpson, R. W. In the shadow of 1857-the ef-

- fect of the Great Ft. Tejon Earthquake on subsequent earthquakes in southern California. *Geophysical Research Letters*, 23 (3):229–232, Feb. 1996. doi: 10.1029/96gl00015.
- Harris, R. A. and Simpson, R. W. Suppression of large earthquakes by stress shadows: A comparison of Coulomb and rate-and-state failure. *Journal of Geophysical Research: Solid Earth*, 103 (B10):24439–24451, Oct. 1998. doi: 10.1029/98jb00793.
- Helmstetter, A. and Shaw, B. E. Relation between stress heterogeneity and aftershock rate in the rate-and-state model. *Journal of Geophysical Research: Solid Earth*, 111(B7), July 2006. doi: 10.1029/2005jb004077.
- Im, K., Avouac, J.-P., Heimisson, E. R., and Elsworth, D. Ridgecrest aftershocks at Coso suppressed by thermal destressing. *Nature*, 595(7865):70–74, June 2021. doi: 10.1038/s41586-021-03601-4.
- Imanishi, K., Ando, R., and Kuwahara, Y. Unusual shallow normal-faulting earthquake sequence in compressional northeast Japan activated after the 2011 off the Pacific coast of Tohoku earthquake. *Geophysical Research Letters*, 39(9), May 2012. doi: 10.1029/2012gl051491.
- Japan Meteorological Agency. The Seismological Bulletin of Japan, 2024. https://www.data.jma.go.jp/svd/eqev/data/bulletin/eqdoc.
- Jia, Z., Wang, X., and Zhan, Z. Multifault Models of the 2019 Ridgecrest Sequence Highlight Complementary Slip and Fault Junction Instability. *Geophysical Research Letters*, 47(17), Sept. 2020. doi: 10.1029/2020gl089802.
- Jin, Z. and Fialko, Y. Finite Slip Models of the 2019 Ridgecrest Earthquake Sequence Constrained by Space Geodetic Data and Aftershock Locations. *Bulletin of the Seismological Society of America*, 110(4):1660–1679, June 2020. doi: 10.1785/0120200060.
- Johnson, P. A., Savage, H., Knuth, M., Gomberg, J., and Marone, C. Effects of acoustic waves on stick-slip in granular media and implications for earthquakes. *Nature*, 451(7174):57–60, Jan. 2008. doi: 10.1038/nature06440.
- Kilb, D., Gomberg, J., and Bodin, P. Triggering of earthquake aftershocks by dynamic stresses. *Nature*, 408(6812):570–574, Nov. 2000. doi: 10.1038/35046046.
- King, G., Stein, R., and Lin, J. Static stress changes and the triggering of earthquakes. Bulletin of the Seismological Society of America, 84(3), 1994. doi: 10.1785/BSSA0840030935.
- Kobayashi, H., Koketsu, K., and Miyake, H. Rupture processes of the 2016 Kumamoto earthquake sequence: Causes for extreme ground motions. *Geophysical Research Letters*, 44(12): 6002–6010, June 2017. doi: 10.1002/2017gl073857.
- Kubo, H., Suzuki, W., Aoi, S., and Sekiguchi, H. Source rupture processes of the 2016 Kumamoto, Japan, earthquakes estimated from strong-motion waveforms. *Earth, Planets and Space*, 68 (1), Oct. 2016. doi: 10.1186/s40623-016-0536-8.
- Liu, C., Lay, T., Brodsky, E. E., Dascher-Cousineau, K., and Xiong, X. Coseismic Rupture Process of the Large 2019 Ridgecrest Earthquakes From Joint Inversion of Geodetic and Seismological Observations. *Geophysical Research Letters*, 46(21):11820–11829, Nov. 2019. doi: 10.1029/2019gl084949.
- Liu, Y., Cui, X., Hu, Y., Zhang, J., and Chen, Y. Integrated Investigation on Heterogeneous Lower Crust Rheology in Kyushu and Afterslip Behavior Following the 2016 Mw7.1 Kumamoto Earthquake. *Geophysical Research Letters*, 51(7), Apr. 2024. doi: 10.1029/2023gl107606.
- Ma, K., Chan, C., and Stein, R. S. Response of seismicity to Coulomb stress triggers and shadows of the 1999 Mw = 7.6 Chi-Chi, Taiwan, earthquake. *Journal of Geophysical Research: Solid Earth*, 110(B5), May 2005. doi: 10.1029/2004jb003389.
- Mai, P. M. and Thingbaijam, K. K. S. SRCMOD: An Online Database

- of Finite-Fault Rupture Models. *Seismological Research Letters*, 85(6):1348–1357, Oct. 2014. doi: 10.1785/0220140077.
- Mallman, E. P. and Parsons, T. A global search for stress shadows. *Journal of Geophysical Research:* Solid Earth, 113(B12), Dec. 2008. doi: 10.1029/2007jb005336.
- Mallman, E. P. and Zoback, M. D. Assessing elastic Coulomb stress transfer models using seismicity rates in southern California and southwestern Japan. *Journal of Geophysical Research: Solid Earth*, 112(B3), Mar. 2007. doi: 10.1029/2005jb004076.
- Mancini, S., Segou, M., Werner, M. J., and Cattania, C. Improving physics-based aftershock forecasts during the 2016–2017
 Central Italy Earthquake Cascade. *Journal of Geophysical Research: Solid Earth*, 124(8):8626–8643, Aug. 2019. doi: 10.1029/2019jb017874.
- Mancini, S., Segou, M., Werner, M. J., and Parsons, T. The Predictive Skills of Elastic Coulomb Rate-and-State Aftershock Forecasts during the 2019 Ridgecrest, California, Earthquake Sequence. *Bulletin of the Seismological Society of America*, 110(4): 1736–1751, June 2020. doi: 10.1785/0120200028.
- Marsan, D. Triggering of seismicity at short timescales following Californian earthquakes. *Journal of Geophysical Research: Solid Earth*, 108(B5), May 2003. doi: 10.1029/2002jb001946.
- Marsan, D. Can coseismic stress variability suppress seismicity shadows? Insights from a rate-and-state friction model. *Journal of Geophysical Research*: *Solid Earth*, 111(B6), June 2006. doi: 10.1029/2005jb004060.
- Marsan, D. and Nalbant, S. S. Methods for Measuring Seismicity Rate Changes: A Review and a Study of How the Mw 7.3 Landers Earthquake Affected the Aftershock Sequence of the Mw 6.1 Joshua Tree Earthquake. Pure and Applied Geophysics, 162 (6–7):1151–1185, June 2005. doi: 10.1007/s00024-004-2665-4.
- Martínez-Garzón, P., Meier, M., Collettini, C., Lanza, F., and Dresen, G. Stress Heterogeneities Governed by Fault Structure and Stress Transfer: The 2016–2017 Central Italy Seismic Sequence. *Journal of Geophysical Research: Solid Earth*, 130(8), Aug. 2025. doi: 10.1029/2024jb029763.
- McCloskey, J., Nalbant, S. S., Steacy, S., Nostro, C., Scotti, O., and Baumont, D. Structural constraints on the spatial distribution of aftershocks. *Geophysical Research Letters*, 30(12), June 2003. doi: 10.1029/2003gl017225.
- Meade, B. J., DeVries, P. M. R., Faller, J., Viegas, F., and Wattenberg, M. What Is Better Than Coulomb Failure Stress? A Ranking of Scalar Static Stress Triggering Mechanisms from 105 Mainshock-Aftershock Pairs. *Geophysical Research Letters*, 44(22), Nov. 2017. doi: 10.1002/2017gl075875.
- Meier, M., Werner, M. J., Woessner, J., and Wiemer, S. A search for evidence of secondary static stress triggering during the 1992 Mw7.3 Landers, California, earthquake sequence. *Journal of Geophysical Research: Solid Earth*, 119(4):3354–3370, Apr. 2014. doi: 10.1002/2013jb010385.
- Meng, X. and Peng, Z. Seismicity rate changes in the Salton Sea Geothermal Field and the San Jacinto Fault Zone after the 2010 Mw 7.2 El Mayor-Cucapah earthquake. *Geophysical Journal International*, 197(3):1750–1762, Apr. 2014. doi: 10.1093/gji/ggu085.
- Michael, A. J. Determination of stress from slip data: Faults and folds. *Journal of Geophysical Research: Solid Earth*, 89(B13): 11517–11526, Dec. 1984. doi: 10.1029/jb089ib13p11517.
- Nakagomi, K., Terakawa, T., Matsumoto, S., and Horikawa, S. Stress and pore fluid pressure control of seismicity rate changes following the 2016 Kumamoto earthquake, Japan. *Earth, Planets and Space*, 73(1), Jan. 2021. doi: 10.1186/s40623-020-01329-5.

- Okada, Y. Internal deformation due to shear and tensile faults in a half-space. *Bulletin of the Seismological Society of America*, 82 (2):1018–1040, Apr. 1992. doi: 10.1785/bssa0820021018.
- Parsons, T. Global Omori law decay of triggered earthquakes: Large aftershocks outside the classical aftershock zone. *Journal of Geophysical Research: Solid Earth*, 107(B9), Sept. 2002. doi: 10.1029/2001jb000646.
- Parsons, T. A hypothesis for delayed dynamic earthquake triggering. *Geophysical Research Letters*, 32(4), Feb. 2005. doi: 10.1029/2004gl021811.
- Parsons, T., Stein, R. S., Simpson, R. W., and Reasenberg, P. A. Stress sensitivity of fault seismicity: A comparison between limited-offset oblique and major strike-slip faults. *Journal of Geophysical Research: Solid Earth*, 104(B9):20183–20202, Sept. 1999. doi: 10.1029/1999jb900056.
- Perfettini, H. and Avouac, J. Postseismic relaxation driven by brittle creep: A possible mechanism to reconcile geodetic measurements and the decay rate of aftershocks, application to the Chi-Chi earthquake, Taiwan. *Journal of Geophysical Research: Solid Earth*, 109(B2), Feb. 2004. doi: 10.1029/2003jb002488.
- Pollitz, F. F. and Cattania, C. Connecting crustal seismicity and earthquake-driven stress evolution in Southern California. *Journal of Geophysical Research: Solid Earth*, 122(8):6473–6490, Aug. 2017. doi: 10.1002/2017jb014200.
- Pollitz, F. F. and Johnston, M. J. S. Direct test of static stress versus dynamic stress triggering of aftershocks. *Geophysical Research Letters*, 33(15), Aug. 2006. doi: 10.1029/2006gl026764.
- Reasenberg, P. A. and Simpson, R. W. Response of Regional Seismicity to the Static Stress Change Produced by the Loma Prieta Earthquake. *Science*, 255(5052):1687–1690, Mar. 1992. doi: 10.1126/science.255.5052.1687.
- Ross, Z. E., Idini, B., Jia, Z., Stephenson, O. L., Zhong, M., Wang, X., Zhan, Z., Simons, M., Fielding, E. J., Yun, S.-H., Hauksson, E., Moore, A. W., Liu, Z., and Jung, J. Hierarchical interlocked orthogonal faulting in the 2019 Ridgecrest earthquake sequence. *Science*, 366(6463):346–351, Oct. 2019. doi: 10.1126/science.aaz0109.
- Sagiya, T., Miyazaki, S., and Tada, T. Continuous GPS Array and Present-day Crustal Deformation of Japan. *Pure and Applied Geophysics*, 157(11):2303–2322, Dec. 2000. doi: 10.1007/pl00022507.
- SCEDC. Southern California Earthquake Data Center, 2013. doi: 10.7909/C3WD3XH1.
- Segou, M. and Parsons, T. The stress shadow problem in physics-based aftershock forecasting: Does incorporation of secondary stress changes help? *Geophysical Research Letters*, 41(11): 3810–3817, June 2014. doi: 10.1002/2013gl058744.
- Segou, M. and Parsons, T. A New Technique to Calculate Earthquake Stress Transfer and to Probe the Physics of Aftershocks. *Bulletin of the Seismological Society of America*, 110(2):863–873, Feb. 2020. doi: 10.1785/0120190033.
- Segou, M., Parsons, T., and Ellsworth, W. Comparative evaluation of physics-based and statistical forecasts in Northern California. *Journal of Geophysical Research: Solid Earth*, 118(12): 6219–6240, Dec. 2013. doi: 10.1002/2013jb010313.
- Sharma, S., Hainzl, S., Zöeller, G., and Holschneider, M. Is Coulomb Stress the Best Choice for Aftershock Forecasting? *Journal of Geophysical Research: Solid Earth*, 125(9), Sept. 2020. doi: 10.1029/2020jb019553.
- Steacy, S., Nalbant, S. S., McCloskey, J., Nostro, C., Scotti, O., and Baumont, D. Onto what planes should Coulomb stress perturbations be resolved? *Journal of Geophysical Research: Solid Earth*, 110(B5), May 2005. doi: 10.1029/2004jb003356.

- Stein, R. S., Barka, A. A., and Dieterich, J. H. Progressive failure on the North Anatolian fault since 1939 by earthquake stress triggering. *Geophysical Journal International*, 128(3):594–604, Mar. 1997. doi: 10.1111/j.1365-246x.1997.tb05321.x.
- Toda, S. and Stein, R. Toggling of seismicity by the 1997 Kagoshima earthquake couplet: A demonstration of time-dependent stress transfer. *Journal of Geophysical Research: Solid Earth*, 108(B12), Dec. 2003. doi: 10.1029/2003jb002527.
- Toda, S. and Stein, R. S. Response of the San Andreas fault to the 1983 Coalinga-Nuñez earthquakes: An application of interaction-based probabilities for Parkfield. *Journal of Geophysical Research: Solid Earth*, 107(B6), June 2002. doi: 10.1029/2001jb000172.
- Toda, S. and Stein, R. S. Central shutdown and surrounding activation of aftershocks from megathrust earthquake stress transfer. *Nature Geoscience*, 15(6):494–500, June 2022. doi: 10.1038/s41561-022-00954-x.
- Toda, S., Stein, R. S., Beroza, G. C., and Marsan, D. After-shocks halted by static stress shadows. *Nature Geoscience*, 5 (6):410–413, May 2012. doi: 10.1038/ngeo1465.
- Uchide, T. Focal mechanisms of small earthquakes beneath the Japanese islands based on first-motion polarities picked using deep learning. *Geophysical Journal International*, 223(3): 1658–1671, Aug. 2020. doi: 10.1093/gji/ggaa401.
- van der Elst, N. J. and Brodsky, E. E. Connecting near-field and far-field earthquake triggering to dynamic strain. *Journal of Geophysical Research: Solid Earth*, 115(B7), July 2010. doi: 10.1029/2009jb006681.
- van der Elst, N. J. and Savage, H. M. Frequency dependence of delayed and instantaneous triggering on laboratory and simulated faults governed by rate-state friction. *Journal of Geophysical Research: Solid Earth*, 120(5):3406–3429, May 2015. doi: 10.1002/2014jb011611.
- Wells, D. L. and Coppersmith, K. J. New empirical relationships among magnitude, rupture length, rupture width, rupture area, and surface displacement. *Bulletin of the Seismological Society of America*, 84(4):974–1002, Aug. 1994. doi: 10.1785/bssa0840040974.
- Woessner, J., Hauksson, E., Wiemer, S., and Neukomm, S. The 1997 Kagoshima (Japan) earthquake doublet: A quantitative analysis of aftershock rate changes. *Geophysical Research Letters*, 31(3), Feb. 2004. doi: 10.1029/2003gl018858.
- Woessner, J., Hainzl, S., Marzocchi, W., Werner, M. J., Lombardi, A. M., Catalli, F., Enescu, B., Cocco, M., Gerstenberger, M. C., and Wiemer, S. A retrospective comparative forecast test on the 1992 Landers sequence. *Journal of Geophysical Research*, 116(B5), May 2011. doi: 10.1029/2010jb007846.
- Xu, X., Sandwell, D. T., and Smith-Konter, B. Coseismic Displacements and Surface Fractures from Sentinel-1 InSAR: 2019 Ridgecrest Earthquakes. *Seismological Research Letters*, 91(4): 1979–1985, Jan. 2020. doi: 10.1785/0220190275.
- Yagi, Y., Okuwaki, R., Enescu, B., Kasahara, A., Miyakawa, A., and Otsubo, M. Rupture process of the 2016 Kumamoto earthquake in relation to the thermal structure around Aso volcano. *Earth, Planets and Space*, 68(1), July 2016. doi: 10.1186/s40623-016-0492-3.
- Yue, C., Dai, D., Li, X., Wang, Y., Zhang, Y., Yang, W., Han, Y., Qu, C., and Meng, L. Aftershock Triggering Mechanism by the 7 January 2025 Mw 7.1 Tingri Earthquake. *Seismological Research Letters*, Sept. 2025. doi: 10.1785/0220250091.
- Yue, H., Ross, Z. E., Liang, C., Michel, S., Fattahi, H., Fielding, E., Moore, A., Liu, Z., and Jia, B. The 2016 Kumamoto Mw = 7.0 Earthquake: A Significant Event in a Fault–Volcano System. *Journal of Geophysical Research: Solid Earth*, 122(11):

- 9166-9183, Nov. 2017. doi: 10.1002/2017jb014525.
- Yue, H., Sun, J., Wang, M., Shen, Z., Li, M., Xue, L., Lu, W., Zhou, Y., Ren, C., and Lay, T. The 2019 Ridgecrest, California earth-quake sequence: Evolution of seismic and aseismic slip on an orthogonal fault system. *Earth and Planetary Science Letters*, 570:117066, Sept. 2021. doi: 10.1016/j.epsl.2021.117066.
- Zhang, Y., Shan, X., Zhang, G., Gong, W., Liu, X., Yin, H., Zhao, D., Wen, S., and Qu, C. Source Model of the 2016 Kumamoto, Japan, Earthquake Constrained by InSAR, GPS, and Strong-Motion Data: Fault Slip under Extensional Stress. *Bulletin of the Seismological Society of America*, 108(5A):2675–2686, Aug. 2018. doi: 10.1785/0120180023.
- Zhang, Y., Zheng, X., Chen, Q., Liu, X., Huang, X., Yang, Y., Xu, Q., and Zhao, J. Automatic Inversion of Rupture Processes of the Foreshock and Mainshock and Correlation of the Seismicity during the 2019 Ridgecrest Earthquake Sequence. *Seismological Research Letters*, 91(3):1556–1566, Mar. 2020. doi: 10.1785/0220190343.
- Zhuang, J., Ogata, Y., and Vere-Jones, D. Stochastic Declustering of Space-Time Earthquake Occurrences. *Journal of the American Statistical Association*, 97(458):369–380, June 2002. doi: 10.1198/016214502760046925.

The article Aftershocks in Stress Shadows are Inconsistent with Modeled Static Coulomb Stress Changes © 2025 by Jeanne L. Hardebeck is licensed under CC BY 4.0.